HHS Public Access

Author manuscript

Am J Ophthalmol. Author manuscript; available in PMC 2018 October 01.

Published in final edited form as:

Am J Ophthalmol. 2017 October ; 182: 180–193. doi:10.1016/j.ajo.2017.08.001.

Diagnostic Capability of Peripapillary 3D Retinal Nerve Fiber Layer Volume for Glaucoma Using Optical Coherence Tomography Volume Scans

Ziad Khoueir[1,2,3], **Firas Jassim**[1,2], **Linda Yi-Chieh Poon**[1,2,4], **Edem Tsikata**[1,2], **Geulah S. Ben-David**[1,2,5], **Yingna Liu**[1], **Eric Shieh**[1,6], **Ramon Lee**[1,7], **Rong Guo**[2,8], **Georgia Papadogeorgou**[9], **Boy Braaf**[1,10], **Huseyin Simavli**[1,2,11], **Christian Que**[1,2,12], **Benjamin J. Vakoc**[1,10], **Brett E. Bouma**[1,10], **Johannes de Boer**[13,14], and **Teresa C. Chen**[1,2]

[1]Harvard Medical School, Boston, MA [2]Massachusetts Eye and Ear Infirmary, Department of Ophthalmology, Glaucoma Service, Boston, MA [3]Beirut Eye Specialist Hospital, Beirut, Lebanon [4]Department of Ophthalmology, Kaohsiung Chang Gung Memorial Hospital, Chang Gung University College of Medicine, Kaohsiung, Taiwan [5]Sackler School of Medicine, Tel Aviv University, Tel Aviv, Israel [6]Jules Stein Eye Institute, David Geffen School of Medicine, University of California, Los Angeles, CA [7]University of Southern California Roski Eye Institute, Department of Ophthalmology, Keck School of Medicine, University of Southern California, Los Angeles, CA [8]Department of Medicine, University of California, Los Angeles, CA [9]Department of Biostatistics, Harvard TH Chan School of Public Health, Boston, MA [10]Wellman Center for Photomedicine, Massachusetts General Hospital, Boston, MA [11]Pamukkale University School of Medicine, Denizli, Turkey [12]University of the East Ramon Magsaysay Memorial Medical Center, Quezon City, Philippines [13]Department of Physics, LaserLaB Amsterdam, Vrije Universiteit, Amsterdam, The Netherlands [14]Department of Ophthalmology, Vrije Universiteit Medical Center, Amsterdam, The Netherlands

Abstract

Purpose—To determine the diagnostic capability of peripapillary 3-dimensional (3D) retinal nerve fiber layer (RNFL) volume measurements from spectral domain optical coherence tomography (OCT) volume scans for open angle glaucoma (OAG).

Design—Assessment of diagnostic accuracy.

Corresponding Author: Teresa C. Chen, M.D., Massachusetts Eye and Ear Infirmary, Glaucoma Service, 243 Charles Street, Boston, MA 02114, Tel: 617-573-6460, Fax: 617-573-3707, Teresa_Chen@meei.harvard.edu.

B. Financial Disclosures: Johannes de Boer Ph.D. Center for Biomedical Optical Coherence Tomography Research and Translation Scientific Advisory Board Chair (Harvard Medical School), licenses to NIDEK, Inc. (Fremont, California), Terumo Corporation (Tokyo, Japan), Ninepoint Medical (Bedford, Massachusetts), Heidelberg Engineering (Heidelberg, Germany). Benjamin J. Vakoc Ph.D. licenses to Terumo Corporation (Tokyo, Japan) and Ninepoint Medical (Bedford, Massachusetts). Brett E. Bouma PhD. licenses to NIDEK, Inc. (Fremont, California), Terumo Corporation (Tokyo, Japan), Ninepoint Medical (Bedford, Massachusetts), Heidelberg Engineering (Heidelberg, Germany).

Other authors do not have any financial conflicts of interest in the design or conduct of the study.

Methods

Setting: Academic clinical setting.

Study population: 180 patients (113 OAG and 67 normal subjects).

Observation procedures: One eye per subject was included. Peripapillary 3D RNFL volumes were calculated for global, quadrant, and sector regions, using four different sized annuli. Peripapillary 2D RNFL thickness circle scans were also obtained.

Main outcome measures: Area under the receiver operating characteristic curve (AUROC) values, sensitivity, specificity, positive and negative predictive values, positive and negative likelihood ratios.

Results—Among all 2D and 3D RNFL parameters, best diagnostic capability was associated with inferior quadrant 3D RNFL volume of the smallest annulus (AUROC curve value 0.977). Otherwise, global 3D RNFL volume AUROC curve values were comparable to global 2D RNFL thickness AUROC curve values for all 4 annuli sizes (p values: 0.0593 to 0.6866). When comparing the 4 annuli sizes for global RNFL volume, the smallest annulus had the best AUROC curve values (p values: 0.0317 to 0.0380). The smallest sized annulus may have the best diagnostic potential partly due to having no areas excluded for being larger than the 6×6 mm square scanned region.

Conclusion—Peripapillary 3D RNFL volume showed excellent diagnostic performance for detecting glaucoma. Peripapillary 3D RNFL volume parameters have the same or better diagnostic capability compared to peripapillary 2D RNFL thickness measurements, although differences were not statistically significant.

INTRODUCTION

Glaucoma is the leading cause of irreversible blindness worldwide. Sixty million people are affected by glaucoma, and the prevalence of glaucoma is increasing with the aging population. By 2020, it is expected that the number of glaucoma patients will be 80 million.[1] Therefore, glaucoma is a global cause of preventable blindness, and early detection is a mainstay of vision preservation.[2–3] Better structural imaging methods hold the potential for improved early detection, because structural damage often precedes irreversible vision loss and can be imaged objectively and quantitatively.

There are many glaucomatous structural changes that can occur before functional vision loss. Glaucoma causes damage to the retinal ganglion cells, their axons, and adjacent glial cells. This damage leads to cupping of the optic nerve head (ONH) and thinning of the retinal nerve fiber layer (RNFL) and ganglion cell layer,[4] and these structural changes have been demonstrated with fundus photography, histology, and optical coherence tomography (OCT).[4–6] Studies have also shown that initial functional visual field alterations may not occur until after approximately 25% to 40% of the retinal ganglion cells have died.[7,8] This is why focusing on more sensitive imaging methods for detecting structural change may be the best way to diagnose glaucoma earlier or to detect disease progression earlier.[8–10]

The most commonly used glaucoma imaging parameter in commercially available spectral domain OCT machines is RNFL thickness, and thinning of the RNFL is a strong indicator of glaucoma.[11–13] Diffuse RNFL defects are the first structural changes in early glaucoma in 50% of cases.[14,15] For focal RNFL defects, a recent study using RNFL maps reported that glaucoma progression more commonly causes an increase in defect area size than defect depth.[16] Current evaluation of glaucomatous RNFL changes relies on the thickness (z axis) and area (x and y axes) of the defects, but little has been published on three-dimensional (3D) RNFL volumetric measurements.

Papers studying 3D RNFL datasets have been limited to the Korean population and have only indirectly measured RNFL volume loss. In one paper, only healthy patients were studied using the 3D OCT-2000 machine (Topcon Inc., Tokyo, Japan). They concluded that RNFL volume measurements may be valuable for the objective and quantitative evaluation of 3D RFNL changes.[17] Since the authors did not have access to the company's original dataset of RNFL thickness measurements, they developed custom-designed software to indirectly calculate RNFL volume for peripapillary circular regions. Another study using the Cirrus HD-OCT machine (Carl Zeiss Meditec Inc., Dublin, CA) indirectly estimated RNFL volume defects by comparing individual RNFL thickness maps with a normative database map, and the region below the reference level was identified as an RNFL defect. In that study, the 3D RNFL defect volume calculation showed better glaucoma diagnostic performance than peripapillary 2D RNFL thickness measurements.[18] To our knowledge, the current paper is the first to directly calculate peripapillary 3D RNFL volume and to evaluate its diagnostic capability in both normal and glaucoma patients in a multiethnic United States population using the Spectralis spectral domain OCT machine (Heidelberg Engineering, Heidelberg, Germany). We also compared the diagnostic capability of 3D RNFL volume measurements with traditional 2D RNFL thickness measurements.

MATERIALS AND METHODS

Participants and examinations

All study subjects were recruited from the Glaucoma Service at the Massachusetts Eye and Ear Infirmary between January 2009 and July 2014, as part of the prospective SIG (Spectral Domain OCT in Glaucoma) Study where patients were imaged with a high-density 3D imaging protocol. The research protocol was approved by the Massachusetts Eye and Ear Infirmary institutional review board. All methods adhered to the tenets of the Declaration of Helsinki for research involving human subjects, and the study was conducted in accordance with Health Insurance Portability and Accountability Act regulations. Informed consent form was obtained from all the subjects participating in the study. All study subjects underwent a complete eye examination by a glaucoma specialist (T.C.C.), and this included history, visual acuity testing, refraction, Goldmann applanation tonometry, slit-lamp biomicroscopy, gonioscopy, ultrasonic pachymetry (PachPen, Accutome Ultrasound Inc., Malvern, Pennsylvania), dilated ophthalmoscopy, stereo disc photography (Visucam Pro NM; Carl Zeiss Meditec, Inc., Dublin, California), visual field (VF) testing (Swedish Interactive Threshold Algorithm 24–2 test of the Humphrey visual field analyzer 750i; Carl

Zeiss Meditec, Inc., Dublin, California), and volume scans using Spectralis OCT (HRA/Spectralis software version 5.4.8.0, Heidelberg Engineering GmbH, Heidelberg, Germany).

Subjects were included if they had a spherical equivalent between −5.0 and +5.0 diopters and a best-corrected visual acuity of 20/40 or better. Only patients with reliable VF testing were included, with less than 33% fixation losses, less than 20% false positive results, and less than 20% false-negative results.

Patients were excluded if they had discernible anterior segment dysgenesis, corneal scarring or opacities, severe non-proliferative or proliferative diabetic retinopathy, VF loss attributable to a non-glaucoma condition, or a dilated pupil diameter of less than 2 mm. Patients with OCT signal strength of less than 15dB (range, 0 to 40) were excluded from the analysis.[19] Additional criteria for determining adequate scan quality were as follows: a clear fundus image with good optic disc and scan area visibility before and during image acquisition, overlay of volume scan visible and without interruptions, and a continuous scan pattern without missing or blank areas.

For the glaucoma patient group, only open angle glaucoma (OAG) patients were included, and this study included patients with primary open angle glaucoma, pigmentary glaucoma, pseudoexfoliation glaucoma, and normal tension glaucoma. Glaucoma patients were defined as having characteristic changes of the ONH with corresponding abnormal VF defects. The VF was considered to be abnormal if 3 or more contiguous test locations in the pattern standard deviation plot were depressed significantly at the $p<0.05$ level, or if 2 or more locations were at the $p<0.05$ level and the other at the $p<0.01$ level. Early defects had to be on the same side of the horizontal meridian, and the VF defect had to corresponded to the optic nerve appearance.[11] VF abnormalities were classified as early (mean deviation [MD] >-6 decibels [dB]), moderate (−12 dB< MD ≤−6 dB), or severe (MD ≤−12 dB).

Normal subjects were those without ocular disease, except for mild cataracts. Normal subjects also had normal VF test results, as defined by a pattern standard deviation of more than 5% and glaucoma hemifield test results within normal limits.[9]

If both eyes were eligible for the study, one eye was selected randomly by using RANDBETWEEN (min,max) function in Microsoft® Office Excel 2007.

Optic nerve and peripapillary volume scan

All spectral domain OCT imaging was performed with dilation using the Spectralis OCT with the automatic real-time (ART) function activated. Additional details of the SD-OCT technique have been described in other papers.[20,21] The ART function was combined with the eye-tracking system to acquire multiple frames at the same scan location.

Volume scans were obtained with a 20×20 degree field centered on the ONH. One-hundred ninety-three sections were taken with the high speed rate and 3 frames for ART. Each volume scan was then processed using an algorithm developed with MATLAB software version 2012a (MathWorks, Inc., Natick, MA). The segmentation algorithm identified the inner limiting membrane (ILM), the posterior border of the RNFL, and the retinal pigmented epithelium (RPE) using edge and intensity information from the 193 images of each volume

scan. The software identified the center of the optic disc using the spatial information provided by the terminations of the RPE/Bruch's membrane (BM) complex, and then determined peripapillary RNFL volume within 4 different sized annuli centered on the ONH. Each peripapillary 3D annulus had a width of 1mm. The smallest Circumpapillary Annulus 1 (CA1) was defined by an inner diameter of 2.5 mm and an outer diameter of 3.5 mm, larger CA2 by diameters of 3 mm and 4 mm, larger CA3 by diameters of 3.5 mm and 4.5 mm, and largest CA4 by diameters of 4 mm and 5 mm (Figure 1). Each annulus was subdivided by quadrants: superior, temporal, inferior and nasal. The inferior and superior quadrants were further subdivided into 4 octants: infero-temporal [TI], infero-nasal [NI], supero-temporal [TS] and supero-nasal [NS]. RNFL volume was computed for the overall annulus, each quadrant, and the 4 octants. A sample output of the MATLAB interface is shown in Figure 2.

For each patient, the 167 Bscans which crossed the 5 mm largest annulus were checked for algorithm artifacts and errors by a glaucoma specialist (ZK). Artifacts were classified into two types: segmentation artifacts and non-segmentation errors. Segmentation artifacts occurred when the algorithm failed to correctly identify the anatomical layers, and these artifacts were further subdivided into three subtypes: misidentification of the ILM, misidentification of the posterior border of the RNFL, and misidentification of the RPE. Non-segmentation errors usually occurred during image acquisition, and these errors were subdivided into three subtypes: cropped images, mirrored images, and bad quality images where segmentation failed because the signal was indistinguishable from the background noise.

The average 2D RNFL thickness values were recorded from the Spectralis RNFL printout and included the following: overall RNFL (360 degrees), quadrant values (i.e. superior, temporal, inferior, nasal), and sector values (i.e. infero-temporal [TI], infero-nasal [NI], supero-temporal [TS] and supero-nasal [NS]).

Statistical analysis

All of the statistical calculations were performed using R Statistical Software version 3.2.3 and the R package AUC version 0.3.0 (Foundation for Statistical Computing, Vienna, Austria). Demographic characteristics of the normal and glaucoma groups were compared using chi-square tests for categorical variables and 2-tailed Student's t tests for continuous variables. Areas under the receiver operating characteristic (AUROC) curves were calculated for the 3D RNFL volume scans for the 4 annuli (i.e. CA1, CA2, CA3, CA4) for overall volume, quadrants, and 4 octants. We also calculated sensitivity, specificity, positive predictive value (PPV), negative predictive value (NPV), positive likelihood ratio (PLR), and negative likelihood ratio (NLR). The cut off value for each variable was calculated by the statistical program automatically, depending on the maximum value of the *Youden index (J)* which is equal to the maximum of *[Sensitivity + Specificity − 1]*. This value corresponded with the point on the ROC curve furthest from the diagonal line.

Pairwise comparisons of ROC curves were performed to determine which 3D RNFL volume annulus or which 2D RNFL thickness value had best diagnostic capability for detecting glaucoma and early glaucoma.

False positive and false negative values were evaluated with respect to the cut-off value. Normal subjects who had RNFL volume values smaller than the cut off value were counted as false positive OCT diagnoses of glaucoma, and OAG patients who had RNFL volume values larger than the cut off were counted as false negatives.

Differences were considered significant at p values <0.05.

RESULTS

Table 1 shows the demographics of the study population. There were 180 study patients with 67 normal subjects and 113 OAG subjects. Of the 113 OAG subjects, 74 patients had primary open angle glaucoma, 18 had normal tension glaucoma, 14 had pseudoexfoliation glaucoma, and 7 had pigmentary glaucoma. Of the 113 OAG subjects, 31 patients had early glaucoma (27.4%). For all 4 annuli sizes, OAG and early OAG patients had lower 3D RNFL volumes compared to normal patients (Table 2) when comparing overall, quadrant, and octant volumes. In particular, when the entire OAG group was compared to the normal group, RNFL volumes were significantly lower for OAG patients for all regions (i.e. overall, quadrant, and octant volumes), except for the nasal quadrant of CA3 and CA4 whose values were similar for OAG and normal patients (p value 0.0574 and p value 0.2461 respectively). When the early OAG subgroup was compared to the normal group, RNFL volumes were also significantly lower for early OAG patients for all regions (i.e. overall, quadrant and octant volumes), except for the nasal quadrants of CA1, CA2, CA3 and CA4 as well as the temporal quadrants of CA3 and CA4 whose values were similar for early OAG and normal patients (p values 0.0511 to 0.5323).

Despite using a high-density 20×20 degree scan area for volume scans, larger 3D annuli sometimes exceeded the 20×20 degree scanned regions. For our study, we excluded 3D circular annuli regions that were outside the scanned region. A larger annulus size is associated with a higher percentage of regions outside the 20×20 scan area (i.e. smallest annulus CA1, 0%; CA2, 1.7% (3 out of 180 patients); CA3, 5.6% (10 out of 180 patients); largest annulus CA4, 7.2% (13 out of 180 patients).

Table 3 shows the diagnostic ability of 3D RNFL volume parameters for distinguishing normal patients from OAG patients and from a subset of early OAG patients (i.e. AUROC curve values and cutoff values). For global RNFL volume, the smallest annulus CA1 (diameters 2.5 mm and 3.5 mm) had the best diagnostic ability (AUROC 0.955, Table 3) compared to the 3 larger annuli (AUROC 0.942 – 0.912, Table 3); however, pairwise comparisons revealed that these differences were only statistically significant for distinguishing normal from OAG patients and not from early OAG patients (i.e. OAG: CA1 versus CA2, CA3, CA4 with p values 0.0380, 0.0380, 0.0317, respectively; early OAG: CA1 versus CA2, CA3, CA4 with p values 0.0544, 0.0663, 0.0812, respectively).

For all OAG patients, we did pairwise comparisons for 3D RNFL volume quadrants in order to see which quadrants had best diagnostic ability (Table 3). Inferior RNFL volume CA1 had the highest AUROC value (0.977), which was significantly better than larger quadrant annuli CA2, CA3 and CA4 (p values 0.0127, 0.0127, and 0.0168, respectively). Smallest annuli

CA1 also had the highest AUROC values in the superior, temporal and nasal quadrants, but pairwise comparisons with the 3 other larger annuli (CA2, CA3, CA4) did not show that CA1 was significantly better. For a subset of early OAG patients, we did pairwise comparisons of RNFL volume quadrants in order to see which quadrants had best diagnostic ability to detect early glaucoma (Table 3). Although the smallest annuli CA1 had the highest AUROC values compared to larger annuli CA2, CA3, and CA4 for all global, quadrant, and octant regions, these differences were not statistically significant.

The diagnostic performance of 3D RNFL volume parameters for distinguishing normals from all OAG patients and early OAG patients is shown in Table 4. In contrast, the diagnostic capability of traditional 2D RNFL thickness measurements for OAG patients is shown in Table 5 and for early OAG patients in Table 6. Best diagnostic abilities for 2D RNFL thickness were associated with the inferior and global values (AUROC curve values 0.966 and 0.959 respectively for all OAG patients [Table 5]; 0.939 and 0.931 respectively for early OAG patients [Table 6]). Therefore, inferior and global 2D RNFL thickness measurements were initially used for pairwise comparisons with inferior and global 3D RNFL volume measurements, using best 3D RNFL annulus CA1.

When comparing the diagnostic ability of inferior and global 2D RNFL thickness (Table 5) to CA1 3D RNFL volume parameters for all OAG patients (Table 3), CA1 inferior 3D RNFL volume had a higher AUROC curve value compared the inferior RNFL thickness (AUROC curve values 0.977 versus 0.966); however, these differences were not statistically significant (p values 0.3292 and 0.6866, respectively). When comparing the diagnostic ability of both inferior and global 2D RNFL thickness to CA1 3D RNFL volume parameters for the subset of early OAG patients (Tables 3 and 6), results were also not significantly different (p values 0.7258 and 0.9501, respectively).

False positive and false negative values were evaluated with respect to the cut-off value. CA1 inferior 3D RNFL volume had the best values for sensitivity and specificity of all 3D RNFL volume parameters (0.93 and 0.97 respectively for all OAG patients [Table 4]). The inferior 2D RNFL thickness had the best values for sensitivity and specificity between all 2D parameters (0.91 and 0.97 respectively for all OAG patients [Table 5]). The percentages of false positives were the same for CA1 inferior 3D RNFL volume and inferior 2D RNFL thickness (1.9% and 1.9%). However, the percentage of false negatives were lower for CA1 inferior 3D RNFL volume compared to inferior 2D RNFL thickness (11.3% versus 13.0%, p value 0.700). When comparing global parameters, the percentage of false positives was higher for CA1 global 3D RNFL compared to global 2D RNFL thickness (3.0% and 2.1%, p value 0.693). However, the percentage of false negatives was lower for CA1 global 3D RNFL volume compared to global 2D RNFL thickness (21.0% versus 23.5%, p value 0.670).

A total of 30,060 images were examined by a glaucoma specialist (ZK) for artifacts. For all 30,060 B-Scans, the total artifact rate was 21.2% (6,361 out of 30,060 images). Cropping occurred in 1.7% of images (510 out of 30,060), mirroring occurred in 0.08% of images (24 out of 30,060), and bad quality in 0.4% of images (126 out of 30,060). Bad quality scans were scans where the signal was indistinguishable from the background noise. Incorrect

segmentation of the ILM occurred in 2.4% of images (709 out of 30,060), incorrect segmentation of the posterior border of the RNFL occurred in 15.2% of images (4,556 out of 30,060), and incorrect segmentation of the RPE/BM complex occurred in 1.4% of images (427 out of 30,060).

In general, there were more artifacts noted in OAG patients compared to normal patients. For OAG patients, the total artifact rate was 24.2% (4,563 out of 18,871). Cropping occurred in 2.1 % of images (388 out of 18,871), mirroring in 0.03% (5 out of 18,871), and bad quality images in 0.6% (109 out of 18,871). Incorrect segmentation of the ILM occurred in 3.2% of images (608 out of 18,871), incorrect posterior RNFL border segmentation in 16.9% (3,196 out of 18,871), and incorrect RPE segmentation in 1.3% (251 out of 18,871). In contrast, for normal patients, the total artifact rate was 16.1% (1,798 out of 11,189). Cropping occurred in 1.1% of images (122 out of 11,189), mirroring in 0.2% (19 out of 11,189), and bad quality images in 0.2% (17 out of 11,189). Incorrect ILM segmentation occurred in 0.9% of images (101 out of 11,189), incorrect posterior RNFL border segmentation in 12.2% of images (1,360 out of 11,189), and incorrect RPE segmentation in 1.6% of images (176 out of 11,189).

DISCUSSION

To our knowledge, this is the first study to show that high-density 3D volume scans which enable direct measurements of 3D RNFL volume have the same or better diagnostic capability (i.e. AUROC curves) for glaucoma when compared to 2D RNFL thickness measurements in a multi-ethnic population; however, these differences were not significantly different (Tables 3 and 5). Also, although the best 3D RNFL volume parameter had fewer or the same rates of false negatives and false positives respectively compared to its corresponding 2D RNFL thickness parameter, differences were also not significant (i.e. false negatives: 11.0% for CA1 inferior 3D RNFL volume versus 13.3% for inferior RNFL thickness, p value 0.700; false positives: both 1.9% for CA1 inferior 3D RNFL volume and inferior 2D RNFL thickness). Our results also show that peripapillary RNFL volume can be used as a diagnostic tool for differentiating glaucoma from normal patients, because glaucoma patients as well as a subset of early glaucoma patients have lower RNFL volume values compared to normal patients for all annuli and sectors (Table 2). Past studies which have indirectly estimated 3D RNFL volume loss support these conclusions but were limited to the Korean population and did not evaluate different annuli sizes for diagnostic capability.[18,22]

The full diagnostic potential of spectral domain OCT has not yet been realized for glaucoma care, because current software does not fully utilize the 3D information that spectral domain OCT technology can acquire. This paper seeks to fill that gap. Commercially available spectral domain OCT machines do not calculate 3D peripapillary RNFL volume but instead calculates 2D RNFL thickness along a peripapillary scan circle. Our 3D study protocol does not utilize a 2D circular scan but instead uses a high-density 3D volume scan with tracker averaging, with a total of 579 frames per volume scan, which enables direct calculation of 3D RNFL volume annuli from raw imaging data. The acquisition times for volume scans are only several more seconds than most peripapillary RNFL circle scan protocols. Shin et al.

reported RNFL volumes in the Korean population using a 128 frame volume scan and did not have access to the machine's raw imaging data, which limits RNFL volume measurements to indirect calculations.[17] Other papers used a normative database of 261 normal Korean patients to build a normative RNFL thickness map. Using MATLAB, the patient's thickness map was then compared to this normative database map to identify the area of RNFL volume defect. Then RNFL "defect volume deviation" was calculated by summing the differences between the normative database and the subject's RNFL measurement to obtain an estimate of RNFL loss. These studies concluded that the volume of diffuse RNFL defects was significantly associated with the severity of glaucomatous damage (p value = 0.009),[18] and that RNFL "defect volume deviation" had significantly greater AUROC values (0.986) than all 2D RNFL thickness parameters (all p values < 0.001).[22] Therefore, the literature suggests that 3D RNFL volume data (either indirect or "defect volume deviation") may have the same or better ability compared to 2D RNFL thickness data.[18,22]

This study demonstrates that direct 3D RNFL volume calculations are possible, and that data can be simply presented in annular regions. Current 2D RNFL software primarily presents data along a peripapillary circular scan. The literature has shown that best 2D RNFL thickness parameters have good diagnostic capability, with AUROC curves ranging between 0.884 and 0.970.[23–26] This study demonstrates that global 3D RNFL volume data has the same diagnostic capability compared to 2D RNFL thickness values (Tables 3 and 5). In the current study, all four 3D RNFL volume annuli had AUROC curve values that were similar to global 2D RNFL thickness (i.e. 0.955, 0.942, 0.928, and 0.912 respectively for CA1 CA2 CA3 and CA4 compared to 0.959 for RNFL thickness; Tables 3 and 5) since the difference was not statistically significant in pair wise comparisons (p values 0.6866, 0.2296, 0.0810 and 0.0593, respectively). Our study, which calculates 3D RNFL volume directly, is consistent with previous reports, which calculated 3D RNFL volume indirectly and which showed that 3D RNFL data has a good diagnostic capability when compared to 2D RNFL thickness.[18,22] Even though these studies[18,22] and the current one suggest that 3D data may be the same or better than 2D RNFL measurements, further studies are needed to demonstrate how 3D RNFL volume data can best depict glaucomatous abnormalities that are missed by 2D RNFL data. Perhaps future 3D RNFL volume studies need to focus not on annular analysis but 3D RNFL mapping, which may be better for detecting both focal and diffuse glaucomatous defects. The most popular commercially available RNFL scan is the circumpapillary RNFL thickness scan, which measures RNFL thickness along a 3.46-mm circle scan only in the z axis and not glaucomatous RNFL damage in all x-y-z directions. Past studies have shown that diffuse RNFL loss is more common than focal RNFL loss, and therefore 3D RNFL data may better detect early glaucomatous damage. For example, Leung et al. demonstrated that the most common patterns found in mild glaucoma were diffuse RNFL loss involving the inferior (20.5%) or both the superior and inferior (20.5%) quadrants whereas localized RNFL defects constituted only 11.4% of defects.[27] Shin et al. also found that 64.1% of RNFL defects were diffuse and of those, 47.7% had mild glaucoma.[18] Shin further noted that circumpapillary RNFL thickness may miss RNFL defects if diffuse RNFL defects exist or deteriorate outside the 3.46 mm diameter scan circle.[18] All these findings together suggest that early detection of diffuse RNFL defects is

more important in early glaucoma than focal defects. By extrapolation, volumetric analysis of RNFL defects warrants more research to detect changes in all x-y-z directions instead of just focal defects along a circular scan.

An advantage of 3D RNFL volume scans over 2D RNFL thickness circular scans is that 3D RFL volume scans are not prone to decentration errors. Since the peripapillary RNFL is normally thinner as one is further away from the optic nerve head, scan decentration of the 2D RNFL scan circle causes artifactual changes in the RNFL thickness values.[28–31] Decentration artifacts are known to occur in about 27.8% of RNFL thickness circular scans.[32] In contrast, 3D RNFL volume scans are more robust and not subject to these measurement errors, because our algorithm automatically determines the center of the ONH.[33–36]

This study also evaluated which 3D RNFL volume quadrants may have the best diagnostic capability, and our results showed that the inferior quadrant of CA1 had the highest AUROC value out of all 2D and 3D RNFL measurements (0.977, Table 3). Inferior quadrant and overall 3D RNFL volume had the highest diagnostic ability for each annulus (Table 3). These findings are similar to circumpapillary 2D RNFL thickness for which overall and inferior thickness measurements provide the best diagnostic capability.[12,18,22–26,37–39] This study also found that 3D RNFL volume had a low diagnostic ability in the nasal quadrant (Table 3) This finding is consistent with the fact that 2D RNFL nasal quadrant has traditionally had the lowest diagnostic capability of the 2D RNFL thickness quadrants.[22,24,25,37–39]

This study also showed that normal RNFL volumes were greater in the superior and inferior quadrants compared to the temporal and nasal quadrants for all four circumpapillary annuli (Table 2). This is similar to RNFL thickness data in healthy eyes where the inferior and superior quadrants were thicker than the nasal and temporal quadrants.[24,37,40] This normal double-hump pattern is a widely accepted RNFL distribution concept[40,41] and was also confirmed in studies of indirect RNFL volume measurements in healthy Korean subjects using spectral domain OCT.[17] Therefore, our study supports the normal “double hump” pattern of the RNFL, and this also supports the validity of our segmentation algorithm. Our customized computer algorithm is further validated by the Shin et al study,[17] whose indirect RNFL volume calculated values were similar to those found for our direct RNFL volume calculated values, although the definitions of annuli regions were slightly different for the two studies. For example, Shin et al noted that the average global RNFL volume between the 2.5 mm and 5 mm circles *indirectly* calculated was 1.478 mm^3, compared to our current study where the global volume between the 2.5 mm to 4.5 mm circles *directly* calculated was 1.018 mm^3 (i.e. combination of CA1 and CA3, Table 2).

Our study also sought to determine which annulus size had the best diagnostic potential, and we found that the smallest annulus size CA1 (2.5mm to 3.5mm) had the best diagnostic capability for two reasons (Figure 1). The first reason is that CA1 was the only annulus that did not have any excluded areas due to being outside the 20×20 degree cube volume scan. For smallest size annulus CA1, there were no subjects excluded, compared to 7.2% (13 of 180 subjects) for largest size annulus CA4 (4mm to 5mm). CA4 had the lowest AUROC

curve value for overall 3D RNFL volume (0.912, Table 3) as well as the lowest sensitivity (81.0%, Table 4). Largest annulus CA4 may have had the lowest AUROC curve values, because it had the highest percentage of excluded regions (7.2%). It is possible that CA4 would have had better diagnostic ability if a larger than 20×20 degree region were obtained, as suggested by our previous paper.[42] It is important to note that the outermost annuli CA4 is the only annulus which does not encompass the traditional 3.4 mm scan circle. Past studies have shown that the 3.4 mm circle carries higher sensitivity to subtle RNFL changes as compared to the 4.5 mm circle that is located in an area where the RNFL is normally thinner.[43] The second reason is that CA1 performs the best in the inferior quadrant, which is known to be the most sensitive quadrant for early glaucoma detection (AUROC value 0.977, Table 3). The smallest annulus CA1 had significantly better diagnostic capability for the inferior quadrant compared to larger annuli CA2, CA3 and CA4 (p values 0.0127, 0.0127, and 0.0168, respectively). Previous reports have shown that localized and diffuse defects in glaucoma predominantly affect the inferior quadrant.[16,44] In moderate to advanced glaucoma, localized RNFL defects constitute 4.2% of the defects, whereas 94.5% demonstrate diffuse defects. In addition to that, diffuse RNFL defects are located closer to the optic disc than localized RNFL defects.[18] According to those findings, our study population that has a large proportion of patients with moderate to advanced glaucoma (72.6%, 82 of 113 subjects) would have a high proportion of diffuse defects predominantly inferiorly and close to the optic nerve which explains why the inferior quadrant of annulus CA1 had the highest diagnostic capability among all 2D and 3D measurements.

In theory, 3D RNFL volume measurements may be less affected by RNFL segmentation artifacts, because incorrect segmentation is more easily corrected by interpolation in 3D datasets than 2D datasets; and this study confirms this hypothesis. In the current study, we analyzed 30,060 B-scans in 3D datasets for algorithm errors in 180 patients, and the posterior border of the RNFL was misidentified in 15.2% of the frames (4,556 out of 30,060 images). Prior studies have of 2D RNFL thickness measurements have reported artifacts rates ranging from 18.0% to 46.7%.[32,45–48] In the current study of 3D RNFL volume, we also found that algorithm failure in segmenting the posterior border of the RNFL was higher in OAG patients (16.9%) compared to normal patients (12.2%), and this is consistent with a previous report from our group.[32] Accurate RNFL thickness measurements are more difficult to obtain in glaucoma patients, because glaucomatous disease causes thinning of the RNFL and also loss of reflectivity of this layer. When there is a decrease in RNFL reflectivity, it is more challenging for automated OCT algorithms to differentiate the posterior RNFL border from the less reflective underlying structures. Therefore, delineating the posterior RNFL border is especially difficult in moderate and severe glaucoma patients, who have more significant loss of RNFL reflectivity.[49] Spectral domain technology offers the possibility to acquire high density volume scans of the ONH with high speed and high resolution. It is known that larger sampling density provides better reproducibility.[50,51] Volume scans are more dense than 2D RNFL scans and have the advantage of offering more sampling over a large area and could be therefore more resistant to the presence of artifacts due to possible interpolation. Further artifact studies are needed to determine how many frames with artifacts can cause clinically significant errors in diagnosis, and best methods to correct these errors need to be developed.

Our study has some limitations. One of the limitations of this study is that all our OAG patients had VF defects. Therefore, this study can only conclude that circumpapillary RNFL volume has diagnostic value for perimetric glaucoma. Further studies are therefore required to evaluate the diagnostic capability of RNFL volume in preperimetric glaucoma. Another potential limitation is the high proportion of moderate to advanced glaucoma patients in our study (72.6%) compared to early glaucoma patients (27.4%). The diagnostic value of structural parameters has more interest in the early stages of the disease since structural RNFL loss is known to precede functional visual field damage.[52,53] Circumpapillary 2D RNFL thickness measurements using spectral domain OCT in normal and glaucoma subjects have been shown to have high reproducibility.[54–56] However, future studies are needed to investigate the reproducibility of peripapillary RNFL volume parameters using our software and segmentation algorithm.

In conclusion, for the detection of both OAG and early OAG patients, 3D peripapillary RNFL volume has similar diagnostic ability as 2D peripapillary RNFL (i.e. AUROC curves). Rates of false positives and false negatives are also similar between 3D RNFL volume and 2D RNFL thickness. Therefore, this study and past literature suggests that best 3D RNFL volume parameters are either the same as or better than 2D RNFL thickness parameters for diagnosing glaucoma,[18,22] although differences may not be significant (Tables 3 and 5). To improve the ability to diagnose glaucoma and to detect disease progression, research on best methods to analyze and present 3D RNFL volume data are needed and should not be limited to 3D RNFL volume annuli data. Such improved tools would better maximize the 3D potential of spectral domain OCT.

Acknowledgments

A. Funding/Support: Teresa C. Chen, M.D. has received funding from the National Institutes of Health UL1 RR 025758, Massachusetts Lions Eye Research Fund, American Glaucoma Society Mid-Career Award, Fidelity Charitable Fund (Harvard University). Boy Braaf Ph.D., Benjamin J. Vakoc Ph.D. and Brett E. Bouma Ph.D. received funding from the Center for Biomedical OCT Research and Translation through Grant Number P41EB015903, awarded by the National Institute of Biomedical Imaging and Bioengineering of the National Institutes of Health.

C. Other Acknowledgements: None

References

1. Quigley HA, Broman AT. The number of people with glaucoma worldwide in 2010 and 2020. Br J Ophthalmol. 2006; 90(3):262–267. [PubMed: 16488940]
2. Thylefors B, Négrel AD. The global impact of glaucoma. Bull World Health Organ. 1994; 72(3): 323–326. [PubMed: 8062393]
3. Chen TC. Spectral domain optical coherence tomography in glaucoma: qualitative and quantitative analysis of the optic nerve head and retinal nerve fiber layer (an AOS thesis). Trans Am Ophthalmol Soc. 2009; 107:254–281. [PubMed: 20126502]
4. Airaksinen PJ, Alanko HI. Effect of retinal nerve fibre loss on the optic nerve head configuration in early glaucoma. Graefes Arch Clin Exp Ophthalmol. 1983; 220(4):193–196. [PubMed: 6884783]
5. Nickells RW. Ganglion cell death in glaucoma: from mice to men. Vet Ophthalmol. 2007; 10(Suppl 1):88–94. [PubMed: 17973839]
6. Schuman JS, Hee MR, Puliafito CA, et al. Quantification of nerve fiber layer thickness in normal and glaucomatous eyes using optical coherence tomography. Arch Ophthalmol. 1995; 113(5):586–596. [PubMed: 7748128]

7. Quigley HA, Addicks EM, Green WR. Optic nerve damage in human glaucoma. III. Quantitative correlation of nerve fiber loss and visual field defect in glaucoma, ischemic neuropathy, papilledema, and toxic neuropathy. Arch Ophthalmol. 1982; 100(1):135–146. [PubMed: 7055464]
8. Kerrigan-Baumrind LA, Quigley HA, Pease ME, Kerrigan DF, Mitchell RS. Number of ganglion cells in glaucoma eyes compared with threshold visual field tests in the same persons. Invest Ophthalmol Vis Sci. 2000; 41(3):741–748. [PubMed: 10711689]
9. Gordon MO, Kass MA. The Ocular Hypertension Treatment Study: design and baseline description of the participants. Arch Ophthalmol. 1999; 117(5):573–583. [PubMed: 10326953]
10. Jaffe GJ, Caprioli J. Optical coherence tomography to detect and manage retinal disease and glaucoma. Am J Ophthalmol. 2004; 137(1):156–169. [PubMed: 14700659]
11. Wu H, de Boer JF, Chen TC. Diagnostic capability of spectral-domain optical coherence tomography for glaucoma. Am J Ophthalmol. 2012; 153(5):815–826.e2. [PubMed: 22265147]
12. Schulze A, Lamparter J, Pfeiffer N, Berisha F, Schmidtmann I, Hoffmann EM. Diagnostic ability of retinal ganglion cell complex, retinal nerve fiber layer, and optic nerve head measurements by Fourier-domain optical coherence tomography. Graefes Arch Clin Exp Ophthalmol. 2011; 249(7): 1039–1045. [PubMed: 21240522]
13. Na JH, Sung KR, Lee JR, et al. Detection of glaucomatous progression by spectral-domain optical coherence tomography. Ophthalmology. 2013; 120(7):1388–1395. [PubMed: 23474248]
14. Tuulonen A, Airaksinen PJ. Initial glaucomatous optic disk and retinal nerve fiber layer abnormalities and their progression. Am J Ophthalmol. 1991; 111(4):485–490. [PubMed: 2012151]
15. Baun O, Møller B, Kessing SV. Evaluation of the retinal nerve fiber layer in early glaucoma. Physiological and pathological findings. Acta Ophthalmol (Copenh). 1990; 68(6):669–673. [PubMed: 2080695]
16. Leung CKS, Choi N, Weinreb RN, et al. Retinal nerve fiber layer imaging with spectral-domain optical coherence tomography: pattern of RNFL defects in glaucoma. Ophthalmology. 2010; 117(12):2337–2344. [PubMed: 20678802]
17. Shin JW, Uhm KB, Seong M, Lee DE. Retinal nerve fiber layer volume measurements in healthy subjects using spectral domain optical coherence tomography. J Glaucoma. 2014; 23(8):567–573. [PubMed: 23970339]
18. Shin JW, Uhm KB, Seong M, Kim YJ. Diffuse retinal nerve fiber layer defects identification and quantification in thickness maps. Invest Ophthalmol Vis Sci. 2014; 55(5):3208–3218. [PubMed: 24744205]
19. Heidelberg Engineering. Spectralis OCT QuickGuide (Software version 5.3). Heidelberg: Heidelberg Engineering; 2010. OCT Acquisition Window1-Overview.
20. Cense B, Nassif N, Chen T, et al. Ultrahigh-resolution high-speed retinal imaging using spectral-domain optical coherence tomography. Opt Express. 2004; 12(11):2435–2447. [PubMed: 19475080]
21. Chen TC, Cense B, Pierce MC, et al. Spectral domain optical coherence tomography: ultra-high speed, ultra-high resolution ophthalmic imaging. Arch Ophthalmol. 2005; 123(12):1715–1720. [PubMed: 16344444]
22. Shin JW, Uhm KB, Seong M. Retinal Nerve Fiber Layer Defect Volume Deviation Analysis Using Spectral Domain Optical Coherence Tomography. Invest Ophthalmol Vis Sci. Dec.2014
23. Kita Y, Kita R, Takeyama A, Takagi S, Nishimura C, Tomita G. Ability of optical coherence tomography-determined ganglion cell complex thickness to total retinal thickness ratio to diagnose glaucoma. J Glaucoma. 2013; 22(9):757–762. [PubMed: 22668980]
24. Rao HL, Zangwill LM, Weinreb RN, Sample PA, Alencar LM, Medeiros FA. Comparison of different spectral domain optical coherence tomography scanning areas for glaucoma diagnosis. Ophthalmology. 2010; 117(9):1692–1699. 1699.e1. [PubMed: 20493529]
25. Oddone F, Centofanti M, Tanga L, et al. Influence of disc size on optic nerve head versus retinal nerve fiber layer assessment for diagnosing glaucoma. Ophthalmology. 2011; 118(7):1340–1347. [PubMed: 21474186]

26. Mwanza J-C, Durbin MK, Budenz DL, et al. Glaucoma diagnostic accuracy of ganglion cell-inner plexiform layer thickness: comparison with nerve fiber layer and optic nerve head. Ophthalmology. 2012; 119(6):1151–1158. [PubMed: 22365056]
27. Leung CK, Cheung CYL, Weinreb RN, et al. Evaluation of retinal nerve fiber layer progression in glaucoma: a study on optical coherence tomography guided progression analysis. Invest Ophthalmol Vis Sci. 2010; 51(1):217–222. [PubMed: 19684001]
28. Vizzeri G, Bowd C, Medeiros FA, Weinreb RN, Zangwill LM. Effect of improper scan alignment on retinal nerve fiber layer thickness measurements using Stratus optical coherence tomograph. J Glaucoma. 2008; 17(5):341–349. [PubMed: 18703942]
29. Vizzeri G, Bowd C, Medeiros FA, Weinreb RN, Zangwill LM. Effect of signal strength and improper alignment on the variability of stratus optical coherence tomography retinal nerve fiber layer thickness measurements. Am J Ophthalmol. 2009; 148(2):249–255.e1. [PubMed: 19427621]
30. Yoo C, Suh IH, Kim YY. The influence of eccentric scanning of optical coherence tomography on retinal nerve fiber layer analysis in normal subjects. Ophthalmologica. 2009; 223(5):326–332. [PubMed: 19478532]
31. Cheung CYL, Yiu CKF, Weinreb RN, et al. Effects of scan circle displacement in optical coherence tomography retinal nerve fibre layer thickness measurement: a RNFL modelling study. Eye (Lond). 2009; 23(6):1436–1441. [PubMed: 18806767]
32. Liu Y, Simavli H, Que CJ, et al. Patient characteristics associated with artifacts in spectralis optical coherence tomography imaging of the retinal nerve fiber layer in glaucoma. Am J Ophthalmol. 2015; 159(3):565–576.e2. [PubMed: 25498118]
33. Garas A, Vargha P, Holló G. Automatic, operator-adjusted, and manual disc-definition for optic nerve head and retinal nerve fiber layer measurements with the RTVue-100 optical coherence tomograph. J Glaucoma. 2011; 20(2):80–86. [PubMed: 20436363]
34. Heidelberg Engineering. How to acquire the perfect image. 2010
35. Lange AP, Sadjadi R, Costello F, Guber I, Traboulsee AL. Reproducibility of retinal nerve fiber layer measurements with manual and automated centration in healthy subjects using spectralis spectral-domain optical coherence tomography. ISRN Ophthalmol. 2012; 2012:860819. [PubMed: 24558593]
36. Carl Zeiss Meditec. Cirrus™ HD-OCT Scan Acquisition Quick Reference Guide. 2012
37. Nakatani Y, Higashide T, Ohkubo S, Takeda H, Sugiyama K. Evaluation of macular thickness and peripapillary retinal nerve fiber layer thickness for detection of early glaucoma using spectral domain optical coherence tomography. J Glaucoma. 2011; 20(4):252–259. [PubMed: 20520570]
38. Na JH, Sung KR, Baek S, Sun JH, Lee Y. Macular and Retinal Nerve Fiber Layer Thickness: Which Is More Helpful in the Diagnosis of Glaucoma? IOVS. 2011; 52(11):8094–8101.
39. Wu H, de Boer JF, Chen TC. Diagnostic capability of spectral-domain optical coherence tomography for glaucoma. Am J Ophthalmol. 2012; 153(5):815–826.e2. [PubMed: 22265147]
40. Varma R, Bazzaz S, Lai M. Optical tomography-measured retinal nerve fiber layer thickness in normal latinos. Invest Ophthalmol Vis Sci. 2003; 44(8):3369–3373. [PubMed: 12882783]
41. Salchow DJ, Oleynikov YS, Chiang MF, et al. Retinal nerve fiber layer thickness in normal children measured with optical coherence tomography. Ophthalmology. 2006; 113(5):786–791. [PubMed: 16650674]
42. Simavli H, Que CJ, Akduman M, et al. Diagnostic Capability of Peripapillary Retinal Thickness in Glaucoma Using 3D Volume Scans. Am J Ophthalmol. 2015; 159(3):545–556.e2. [PubMed: 25498354]
43. Schuman JS, Pedut-Kloizman T, Hertzmark E, et al. Reproducibility of nerve fiber layer thickness measurements using optical coherence tomography. Ophthalmology. 1996; 103(11):1889–1898. [PubMed: 8942887]
44. Shin JW, Uhm KB, Lee WJ, Kim YJ. Diagnostic ability of retinal nerve fiber layer maps to detect localized retinal nerve fiber layer defects. Eye (Lond). 2013; 27(9):1022–1031. [PubMed: 23743523]
45. Leal-Fonseca M, Rebolleda G, Oblanca N, Moreno-Montañes J, Muñoz-Negrete FJ. A comparison of false positives in retinal nerve fiber layer, optic nerve head and macular ganglion cell-inner

plexiform layer from two spectral-domain optical coherence tomography devices. Graefes Arch Clin Exp Ophthalmol. 2013; 252(2):321–330. [PubMed: 24337431]

46. Asrani S, Essaid L, Alder BD, Santiago-Turla C. Artifacts in Spectral-Domain Optical Coherence Tomography Measurements in Glaucoma. JAMA Ophthalmol. Feb.2014
47. Moreno-Montañés J, Antón A, Olmo N, et al. Misalignments in the retinal nerve fiber layer evaluation using cirrus high-definition optical coherence tomography. J Glaucoma. 2011; 20(9): 559–565. [PubMed: 21336154]
48. Kim NR, Lim H, Kim JH, Rho SS, Seong GJ, Kim CY. Factors Associated with False Positives in Retinal Nerve Fiber Layer Color Codes from Spectral-Domain Optical Coherence Tomography. Ophthalmology. 2011; 118(9):1774–1781. [PubMed: 21550120]
49. van der Schoot J, Vermeer KA, Boer JF de, Lemij HG. The Effect of Glaucoma on the Optical Attenuation Coefficient of the Retinal Nerve Fiber Layer in Spectral Domain Optical Coherence Tomography Images. IOVS. 2012; 53(4):2424–2430.
50. Budenz DL, Chang RT, Huang X, Knighton RW, Tielsch JM. Reproducibility of retinal nerve fiber thickness measurements using the stratus OCT in normal and glaucomatous eyes. Invest Ophthalmol Vis Sci. 2005; 46(7):2440–2443. [PubMed: 15980233]
51. Gurses-Ozden R, Ishikawa H, Hoh ST, et al. Increasing sampling density improves reproducibility of optical coherence tomography measurements. J Glaucoma. 1999; 8(4):238–241. [PubMed: 10464731]
52. Sommer A, Katz J, Quigley HA, et al. Clinically detectable nerve fiber atrophy precedes the onset of glaucomatous field loss. Arch Ophthalmol. 1991; 109(1):77–83. [PubMed: 1987954]
53. Quigley HA, Katz J, Derick RJ, Gilbert D, Sommer A. An evaluation of optic disc and nerve fiber layer examinations in monitoring progression of early glaucoma damage. Ophthalmology. 1992; 99(1):19–28. [PubMed: 1741133]
54. Leung CK-S, Cheung CY-L, Weinreb RN, et al. Retinal nerve fiber layer imaging with spectral-domain optical coherence tomography: a variability and diagnostic performance study. Ophthalmology. 2009; 116(7):1257–1263. 1263–2. [PubMed: 19464061]
55. Pierro L, Gagliardi M, Iuliano L, Ambrosi A, Bandello F. Retinal nerve fiber layer thickness reproducibility using seven different OCT instruments. Invest Ophthalmol Vis Sci. 2012; 53(9): 5912–5920. [PubMed: 22871835]
56. Ghasia FF, El-Dairi M, Freedman SF, Rajani A, Asrani S. Reproducibility of spectral-domain optical coherence tomography measurements in adult and pediatric glaucoma. J Glaucoma. 2015; 24(1):55–63. [PubMed: 23722865]

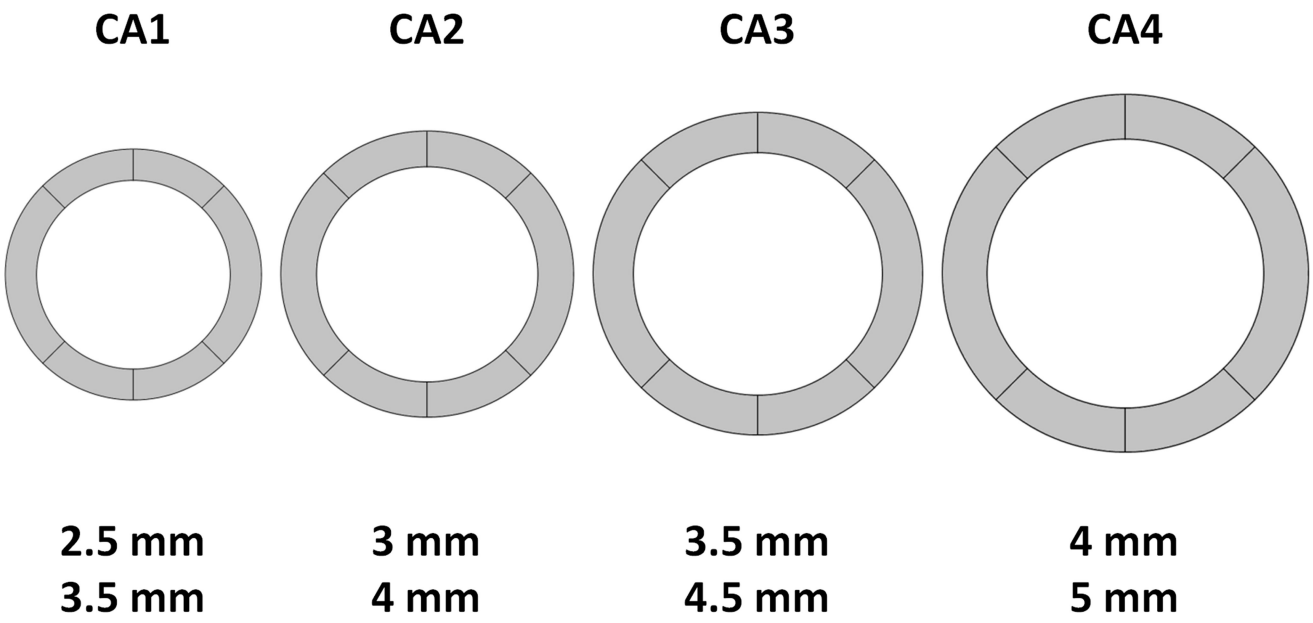

Figure 1.

Diagram of the 4 different size annuli used for peripapillary 3D retinal nerve fiber layer volume determinations using 3D volume scans. The first circumpapillary annulus (CA1) has diameters of 2.5 mm and 3.5 mm; the second circumpapillary annulus (CA2) has diameters of 3 mm and 4 mm; the third circumpapillary annulus (CA3) has diameters of 3.5 mm and 4.5 mm; the fourth circumpapillary annulus (CA4) has diameters of 4 mm and 5 mm.

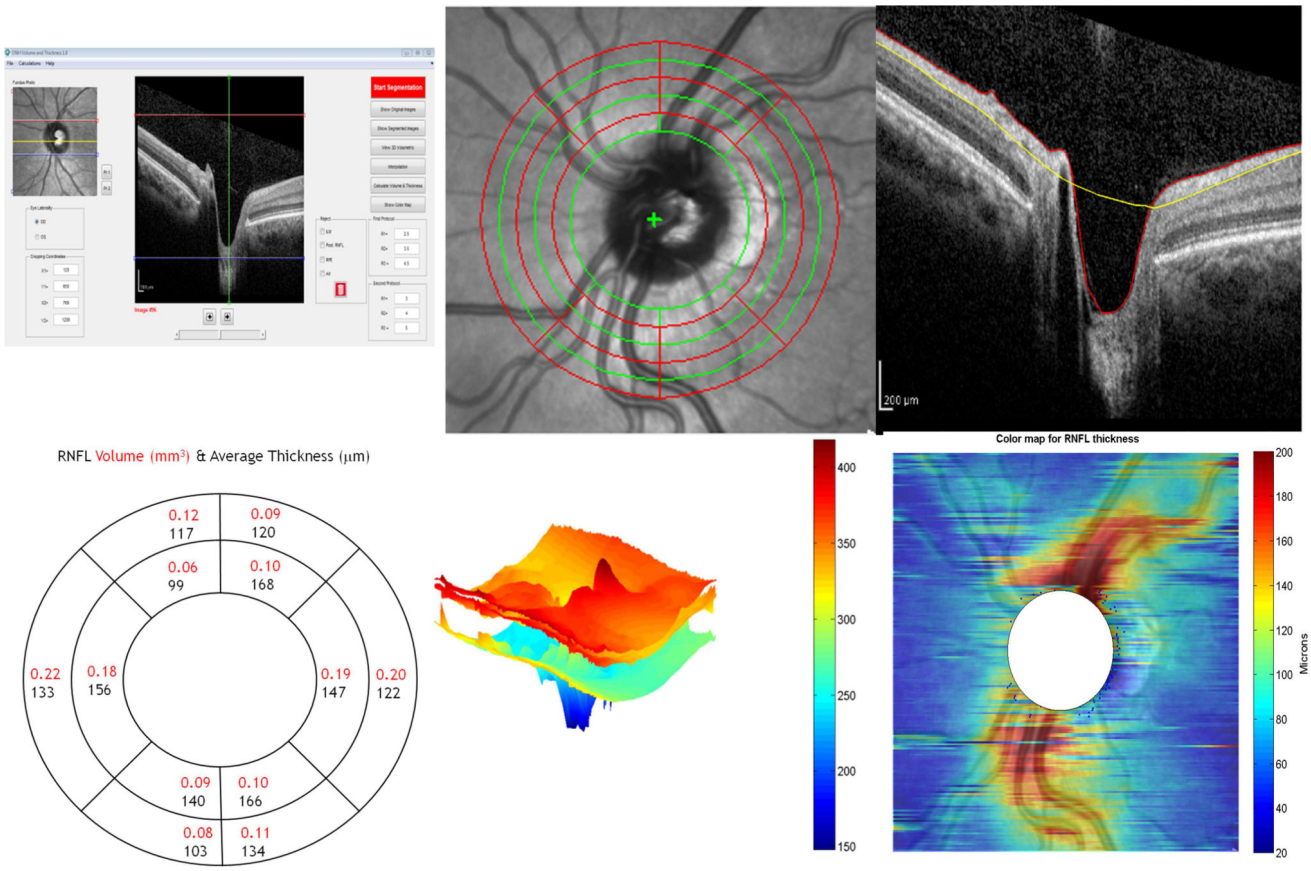

Figure 2.

This figure shows the user interface (top left) and sample output (rest of figures) of the custom-built software used to determine the circumpapillary 3D retinal nerve fiber layer (RNFL) volume from spectral domain optical coherence tomography volume scans. The top middle picture shows how the software defines 4 annuli by superimposing 6 circles on the infrared reflectance (IR) image of the 3D volume scans. The center of the circles is automatically determined as the center of the disc, which is defined by the termination of the retinal pigment epithelium/Bruch's membrane (RPE/BM) complex of the corresponding frames. The top right picture illustrates one of the B scans of the 3D volume set which is automatically segmented using edge and intensity information, and this sample picture represents the 96th image of the 193 B scan volume set. The red line given by the algorithm corresponds to the internal limiting membrane, and the yellow line delineates the posterior border of the retinal nerve fiber layer. Using the information provided by these two lines, the software calculates the average RNFL thickness as well as the RNFL volume for each annulus and its subdivisions. The bottom left picture illustrates a sample average thickness and volume map for circumpapillary annuli 1 and 2. Values for RNFL volume are indicated in red, and average RNFL thickness is indicated in black. The bottom middle figure depicts a 3D map of the peripapillary area and shows the planes of the internal limiting membrane (ILM), the posterior border of the RNFL, and the RPE/BM complex. The bottom right output depicts an RNFL thickness topography map for the 20×20 degree scanned area.

Table 1

Demographics of the normal and open angle glaucoma patients who were imaged with three-dimensional spectral domain optical coherence tomography volume scans.

	Normal	OAG	p^a	Early OAG	p^b
Number of eyes	67	113		31	
Number of right eyes/left eyes	31/36	63/50	0.256	21/11	0.083
Mean age (year)	53.98 ± 16.54	67.86 ± 12.09	<0.0001	68.82 ± 9.66	<0.0001
Refractive error (diopters)					
Sphere	−0.11 ± 1.86	−0.26 ± 1.78	0.617	0.155 ± 1.46	0.488
Cylinder	−0.70 ± 0.78	−0.82 ± 0.80	0.350	−0.83 ± 0.82	0.538
Spherical equivalent	−0.46 ± 1.86	−0.67 ± 1.84	0.492	−0.26 ± 1.60	0.591
Visual Field					
Mean deviation (decibels)	−1.40 ± 1.90	−12.56 ± 7.73	<0.0001	−3.80 ± 1.52	<0.0001
Pattern standard deviation	1.50 ± 0.28	8.51 ± 3.41	<0.0001	4.99 ± 1.86	<0.0001

OAG = open angle glaucoma.

Results are expressed as the mean ± standard deviation unless otherwise indicated.

[a]Normal versus OAG.

[b]Normal versus early OAG.

Table 2

Three-dimensional (3D) retinal nerve fiber layer volume measurements for normal and open angle glaucoma patients: 4 different circumpapillary annuli sizes from 3D spectral domain optical coherence tomography volume scans.

		OAG		Early OAG	
	Mean ± SD (mm^3)	**Mean ± SD (mm^3)**	***p*^a**	**Mean ± SD (mm^3)**	***p*^b**
CA1 (2.5mm – 3.5mm)					
Global	0.494 ± 0.055	0.369 ± 0.053	<0.0001	0.397 ± 0.047	<0.0001
Superior	0.149 ± 0.021	0.102 ± 0.021	<0.0001	0.116 ± 0.019	<0.0001
Inferior	0.153 ± 0.021	0.095 ± 0.020	<0.0001	0.108 ± 0.021	<0.0001
Nasal	0.096 ± 0.033	0.091 ± 0.016	0.0078	0.092 ± 0.015	0.1701
Temporal	0.097 ± 0033	0.082 ± 0.023	0.0004	0.082 ± 0.014	0.0178
NS	0.074 ± 0.014	0.050 ± 0.012	<0.0001	0.058 ± 0.014	<0.0001
TS	0.075 ± 0.012	0.052 ± 0.012	<0.0001	0.058 ± 0.012	<0.0001
TI	0.076 ± 0.014	0.047 ± 0.012	<0.0001	0.054 ± 0.014	<0.0001
NI	0.076 ± 0.012	0.048 ± 0.011	<0.0001	0.054 ± 0.011	<0.0001
CA2 (3mm – 4mm)					
Global	0.511 ± 0.064	0.388 ± 0.058	<0.0001	0.416 ± 0.058	<0.0001
Superior	0.151 ± 0.021	0.107 ± 0.020	<0.0001	0.121 ± 0.020	<0.0001
Inferior	0.155 ± 0.021	0.100 ± 0.022	<0.0001	0.113 ± 0.029	<0.0001
Nasal	0.100 ± 0.014	0.093 ± 0.017	0.0050	0.095 ± 0.016	0.2008
Temporal	0.105 ± 0.044	0.087 ± 0.027	0.0008	0.086 ± 0.016	0.0252
NS	0.075 ± 0.016	0.052 ± 0.013	<0.0001	0.058 ± 0.016	<0.0001
TS	0.076 ± 0.015	0.055 ± 0.012	<0.0001	0.063 ± 0.012	<0.0001
TI	0.078 ± 0.016	0.050 ± 0.013	<0.0001	0.057 ± 0.016	<0.0001
NI	0.078 ± 0.015	0.051 ± 0.013	<0.0001	0.056 ± 0.017	<0.0001
CA3 (3.5mm – 4.5mm)					
Global	0.524 ± 0.069	0.411 ± 0.066	<0.0001	0.432 ± 0.066	<0.0001
Superior	0.151 ± 0.019	0.113 ± 0.020	<0.0001	0.124 ± 0.019	<0.0001

		OAG		Early OAG	
	Mean ± SD (mm^3)	**Mean ± SD (mm^3)**	***p*[a]**	**Mean ± SD (mm^3)**	***p*[b]**
Inferior	0.157 ± 0.021	0.106 ± 0.025	<0.0001	0.118 ± 0.039	<0.0001
Nasal	0.104 ± 0.018	0.098 ± 0.018	0.0574	0.099 ± 0.018	0.3528
Temporal	0.110 ± 0.051	0.093 ± 0.030	0.0061	0.091 ± 0.017	0.0511
NS	0.076 ± 0.019	0.055 ± 0.013	<0.0001	0.059 ± 0.016	<0.0001
TS	0.075 ± 0.017	0.058 ± 0.013	<0.0001	0.065 ± 0.013	0.0046
TI	0.078 ± 0.017	0.052 ± 0.013	<0.0001	0.060 ± 0.017	<0.0001
NI	0.079 ± 0.019	0.054 ± 0.016	<0.0001	0.059 ± 0.026	<0.0001
CA4 (4mm – 5mm)					
Global	0.538 ± 0.076	0.438 ± 0.077	<0.0001	0.450 ± 0.068	<0.0001
Superior	0.153 ± 0.018	0.120 ± 0.021	<0.0001	0.129 ± 0.019	<0.0001
Inferior	0.160 ± 0.021	0.114 ± 0.029	<0.0001	0.123 ± 0.040	<0.0001
Nasal	0.107 ± 0.021	0.103 ± 0.020	0.2461	0.103 ± 0.018	0.5323
Temporal	0.115 ± 0.057	0.101 ± 0.034	0.0364	0.096 ± 0.019	0.0807
NS	0.077 ± 0.019	0.058 ± 0.014	<0.0001	0.061 ± 0.016	0.0002
TS	0.076 ± 0.017	0.062 ± 0.014	<0.0001	0.068 ± 0.014	0.0322
TI	0.079 ± 0.019	0.056 ± 0.014	<0.0001	0.062 ± 0.018	<0.0001
NI	0.082 ± 0.021	0.058 ± 0.019	<0.0001	0.061 ± 0.028	<0.0001

CA1 = circumpapillary annulus 1; CA2 = circumpapillary annulus 2; CA3 = circumpapillary annulus 3; CA4 = circumpapillary annulus 4; NI=infero-nasal; NS=supero-nasal; OAG = open angle glaucoma; SD= standard deviation; TI=infero-temporal; TS=supero-temporal.

[a]Normal versus OAG.

[b]Normal versus early OAG.

Table 3

Diagnostic capability of retinal nerve fiber layer 3D volume scans for open angle glaucoma: areas under the receiver operating characteristic curves and cutoff values for normal versus open angle glaucoma patients who had 3D spectral domain optical coherence tomography volume scans.

	Normal versus OAG		Normal versus Early OAG	
	AUROC (SE)	**Cutoff mm3 (≤)**	**AUROC (SE)**	**Cutoff mm3 (≤)**
CA1 (2.5mm – 3.5mm)				
Global	0.955 (0.015)	0.422	0.929 (0.032)	0.437
Superior	0.941 (0.016)	0.119	0.878 (0.037)	0.128
Inferior	0.977 (0.010)	0.119	0.930 (0.035)	0.119
Nasal	0.661 (0.040)	0.085	0.612 (0.070)	0.086
Temporal	0.805 (0.033)	0.082	0.762 (0.061)	0.083
NS	0.899 (0.023)	0.059	0.805 (0.048)	0.070
TS	0.910 (0.021)	0.058	0.838 (0.043)	0.069
TI	0.945 (0.017)	0.057	0.880 (0.043)	0.061
NI	0.952 (0.013)	0.060	0.912 (0.029)	0.062
CA2 (3mm – 4mm)				
Global	0.942 (0.018)	0.447	0.903 (0.040)	0.458
Superior	0.930 (0.018)	0.119	0.841 (0.043)	0.145
Inferior	0.970 (0.012)	0.127	0.912 (0.041)	0.128
Nasal	0.662 (0.040)	0.088	0.613 (0.069)	0.088
Temporal	0.813 (0.032)	0.090	0.776 (0.062)	0.089
NS	0.871 (0.027)	0.058	0.769 (0.052)	0.073
TS	0.852 (0.027)	0.065	0.744 (0.052)	0.069
TI	0.918 (0.022)	0.062	0.834 (0.049)	0.062
NI	0.923 (0.019)	0.056	0.867 (0.042)	0.068
CA3 (3.5mm – 4.5mm)				
Global	0.928 (0.021)	0.463	0.896 (0.042)	0.475
Superior	0.915 (0.020)	0.132	0.834 (0.045)	0.133
Inferior	0.964 (0.014)	0.130	0.908 (0.043)	0.130
Nasal	0.624 (0.043)	0.102	0.601 (0.068)	0.097
Temporal	0.778 (0.035)	0.094	0.751 (0.0.65)	0.094
NS	0.827 (0.035)	0.059	0.748 (0.054)	0.056
TS	0.789 (0.035)	0.066	0.672 (0.057)	0.074
TI	0.883 (0.024)	0.064	0.796 (0.052)	0.070
NI	0.885 (0.025)	0.062	0.842 (0.044)	0.070
CA4 (4mm – 5mm)				
Global	0.912 (0.024)	0.470	0.882 (0.045)	0.481

	Normal versus OAG		Normal versus Early OAG	
	AUROC (SE)	Cutoff mm3 (≤)	AUROC (SE)	Cutoff mm3 (≤)
Superior	0.893 90.024)	0.139	0.818 (0.049)	0.138
Inferior	0.943 (0.018)	0.136	0.902 (0.044)	0.132
Nasal	0.584 (0.045)	0.103	0.589 (0.067)	0.104
Temporal	0.734 (0.037)	0.102	0.743 (0.067)	0.097
NS	0.803 (0.035)	0.057	0.733 (0.057)	0.057
TS	0.725 (0.042)	0.083	0.628 (0.061)	0.082
TI	0.835 (0.032)	0.072	0.754 (0.055)	0.072
NI	0.838 (0.031)	0.074	0.816 (0.047)	0.074

AUROC=area under the receiver operating characteristic curve; CA1=circumpapillary annulus 1; CA2=circumpapillary annulus 2; CA3= circumpapillary annulus 3; CA4=circumpapillary annulus 4; NI=infero-nasal; NS=supero-nasal; OAG= open-angle glaucoma; SE=standard error ;TI=infero-temporal; TS=supero-temporal.

Table 4

Diagnostic performance of peripapillary 3D retinal nerve fiber layer volume scans for open angle glaucoma and early open angle glaucoma: table of best sensitivity and specificity values for 4 different size circumpapillary annuli derived from 3D spectral domain optical coherence tomography volume scans.

	OAG						Early OAG					
	Sensitivity (CI)	**Specificity (CI)**	**PLR (CI)**	**NLR (CI)**	**PPV(CI)**	**NPV (CI)**	**Sensitivity (CI)**	**Specificity (CI)**	**PLR (CI)**	**NLR (CI)**	**PPV (CI)**	**NPV (CI)**
CA1 (2.5mm – 3.5mm)												
Global	0.85	0.96	18.97	0.16	0.97	0.79	0.9	0.86	6.52	0.11	0.76	0.95
Superior	0.82	0.93	11.03	0.19	0.95	0.76	0.74	0.85	4.82	0.31	0.7	0.87
Inferior	0.93	0.97	31.13	0.07	0.98	0.89	0.81	0.97	26.21	0.2	0.93	0.91
Nasal	0.45	0.88	3.78	0.62	0.86	0.49	0.48	0.83	2.86	0.62	0.58	0.77
Temporal	0.65	0.91	7.31	0.38	0.93	0.61	0.71	0.86	5.13	0.34	0.71	0.86
NS	0.77	0.9	7.37	0.26	0.93	0.7	0.9	0.63	2.45	0.15	0.54	0.93
TS	0.73	0.97	24.31	0.28	0.98	0.68	0.9	0.66	2.67	0.15	0.56	0.93
TI	0.82	0.94	13.79	0.19	0.96	0.76	0.81	0.86	5.82	0.22	0.74	0.9
NI	0.83	0.93	11.15	0.18	0.95	0.77	0.77	0.88	6.29	0.26	0.75	0.89
CA2 (3mm – 4mm)												
Global	0.88	0.91	9.85	0.13	0.94	0.82	0.9	0.83	5.32	0.12	0.71	0.95
Superior	0.75	1	Inf	0.25	1	0.71	0.93	0.57	2.17	0.12	0.5	0.95
Inferior	0.93	0.93	12.45	0.08	0.95	0.89	0.84	0.91	9.09	0.18	0.81	0.92
Nasal	0.44	0.87	3.26	0.65	0.84	0.48	0.45	0.86	3.26	0.64	0.61	0.77
Temporal	0.74	0.84	4.53	0.31	0.88	0.66	0.74	0.85	4.82	0.31	0.7	0.87
NS	0.74	0.87	5.5	0.3	0.9	0.67	0.87	0.55	1.94	0.24	0.47	0.9
TS	0.81	0.78	3.62	0.24	0.86	0.71	0.77	0.66	2.27	0.35	0.51	0.86
TI	0.88	0.87	6.52	0.14	0.92	0.81	0.77	0.86	5.59	0.26	0.73	0.89
NI	0.73	0.96	16.4	0.28	0.97	0.68	0.9	0.71	3.09	0.14	0.6	0.94
CA3 (3.5mm – 4.5mm)												
Global	0.87	0.9	9.13	0.14	0.94	0.8	0.9	0.8	4.58	0.12	0.69	0.94
Superior	0.81	0.9	7.74	0.21	0.93	0.74	0.67	0.88	5.42	0.38	0.71	0.85

	OAG						Early OAG					
	Sensitivity (CI)	**Specificity (CI)**	**PLR (CI)**	**NLR (CI)**	**PPV(CI)**	**NPV (CI)**	**Sensitivity (CI)**	**Specificity (CI)**	**PLR (CI)**	**NLR (CI)**	**PPV (CI)**	**NPV (CI)**
Inferior	0.93	0.91	10.38	0.08	0.95	0.88	0.87	0.91	9.44	0.14	0.82	0.94
Nasal	0.7	0.57	1.63	0.53	0.74	0.52	0.58	0.67	1.77	0.62	0.47	0.76
Temporal	0.72	0.84	4.37	0.34	0.88	0.64	0.74	0.83	4.35	0.31	0.68	0.87
NS	0.71	0.81	3.65	0.36	0.86	0.63	0.53	0.88	4.33	0.53	0.67	0.8
TS	0.78	0.69	2.49	0.32	0.8	0.66	0.8	0.52	1.68	0.38	0.44	0.85
TI	0.85	0.79	4.07	0.19	0.87	0.76	0.9	0.69	2.94	0.14	0.58	0.94
NI	0.83	0.78	3.72	0.22	0.86	0.73	0.9	0.68	2.8	0.14	0.57	0.94
CA4 (4mm – 5mm)												
Global	0.81	0.93	11.31	0.21	0.95	0.73	0.8	0.85	5.4	0.23	0.75	0.88
Superior	0.84	0.83	5.04	0.19	0.9	0.75	0.73	0.83	4.25	0.32	0.69	0.86
Inferior	0.9	0.93	12.07	0.11	0.95	0.85	0.84	0.94	13.63	0.17	0.87	0.92
Nasal	0.56	0.64	1.57	0.68	0.73	0.45	0.61	0.61	1.57	0.63	0.45	0.75
Temporal	0.68	0.76	2.83	0.43	0.82	0.59	0.71	0.86	5.13	0.34	0.71	0.86
NS	0.58	0.92	7.02	0.45	0.93	0.56	0.47	0.91	5.41	0.58	0.74	0.77
TS	0.94	0.45	1.72	0.13	0.75	0.82	0.87	0.45	1.57	0.3	0.45	0.87
TI	0.91	0.66	2.65	0.14	0.81	0.81	0.87	0.66	2.57	0.2	0.55	0.91
NI	0.92	0.63	2.46	0.13	0.8	0.82	0.94	0.62	2.43	0.1	0.54	0.95

CA1=circumpapillary annulus 1; CA2= circumpapillary annulus 2; CA3= circumpapillary annulus 3; CA4= circumpapillary annulus 4; NI=infero-nasal; NLR=negative likelihood ratio; NS=supero-nasal; NPV=negative predictive value; OAG= open-angle glaucoma; PLR=positive likelihood ratio; PPV =positive predictive value; TI=infero-temporal; TS=supero-temporal.

Table 5

Diagnostic performance of two-dimensional retinal nerve fiber layer (RNFL) thickness for open angle glaucoma: table of best sensitivity and specificity values of overall RNFL, RNFL quadrants, and RNFL sectors obtained from spectral domain optical coherence tomography scans.

	AUROC (SE)	Sensitivity (CI)	Specificity (CI)	PLR (CI)	NLR (CI)	PPV (CI)	NPV (CI)
Global	0.959 (0.013)	0.82 (0.74–0.89)	0.97 (0.90–1.00)	27.52 (7.01–108.05)	0.18 (0.12–0.27)	0.98 (0.93–1.00)	0.76 (0.66–0.85)
Superior	0.937 (0.017)	0.81 (0.73–0.88)	0.93 (0.83–0.98)	10.89 (4.66–25.42)	0.20 (0.14–0.30)	0.95 (0.88–0.98)	0.75 (0.64–0.84)
Inferior	0.966 (0.012)	0.91 (0.84–0.96)	0.97 (0.90–1.00)	30.51 (7.78–119.62)	0.09 (0.05–0.17)	0.98 (0.93–1.00)	0.87 (0.77–0.93)
Nasal	0.829 (0.031)	0.87 (0.79–0.92)	0.66 (0.53–0.77)	2.52 (1.80–3.54)	0.20 (0.12–0.34)	0.81 (0.73–0.87)	0.75 (0.62–0.85)
Temporal	0.854 (0.029)	0.76 (0.67–0.83)	0.88 (0.78–0.95)	6.34 (3.29–12.28)	0.27 (0.19–0.38)	0.91 (0.84–0.96)	0.69 (0.58–0.78)
NS	0.869 (0.026)	0.65 (0.56–0.74)	0.93 (0.83–0.98)	8.73 (3.72–20.52)	0.38 (0.29–0.49)	0.94 (0.86–0.98)	0.61 (0.51–0.71)
TS	0.933 (0.019)	0.90 (0.82–0.94)	0.87 (0.76–0.94)	6.65 (3.61–12.25)	0.12 (0.07–0.21)	0.92 (0.85–0.96)	0.83 (0.72–0.91)
TI	0.965 (0.013)	0.95 (0.89–0.98)	0.93 (0.83–0.98)	12.68 (5.45–29.50)	0.06 (0.03–0.13)	0.96 (0.90–0.99)	0.91 (0.82–0.97)
NI	0.905 (0.021)	0.74 (0.65–0.82)	0.91 (0.82–0.97)	8.28 (3.83–17.90)	0.28 (0.21–0.39)	0.93 (0.86–0.97)	0.67 (0.57–0.77)

AUROC=area under receiver operating characteristic curve; CI=95% confidence interval; NI=infero-nasal; NLR=negative likelihood ratio; NPV=negative predictive value; NS=supero-nasal; PLR=positive likelihood ratio; PPV=positive predictive value; SE=standard error; TI=infero-temporal; TS=supero-temporal.

Table 6

Diagnostic performance of two-dimensional retinal nerve fiber layer (RNFL) thickness for early open angle glaucoma: table of best sensitivity and specificity values of overall RNFL, RNFL quadrants, and RNFL sectors obtained from spectral domain optical coherence tomography scans.

	AUROC (SE)	Sensitivity (CI)	Specificity (CI)	PLR (CI)	NLR (CI)	PPV (CI)	NPV (CI)
Global	0.931 (0.025)	0.90 (0.74–0.98)	0.82 (0.70–0.90)	4.89 (2.90–8.26)	0.12 (0.04–0.35)	0.70 (0.53–0.83)	0.95 (0.85–0.99)
Superior	0.878 (0.036)	0.77 (0.59–0.90)	0.85 (0.74–0.92)	5.03 (2.76–9.18)	0.27 (0.14–0.52)	0.71 (0.53–0.85)	0.89 (0.78–0.95)
Inferior	0.939 (0.029)	0.87 (0.70–0.96)	0.94 (0.85–0.98)	14.15 (5.42–36.93)	0.14 (0.06–0.34)	0.87 (0.70–0.96)	0.94 (0.85–0.98)
Nasal	0.755 (0.054)	0.84 (0.66–0.95)	0.66 (0.53–0.77)	2.48 (1.70–3.60)	0.24 (0.11–0.55)	0.54 (0.39–0.69)	0.90 (0.77–0.97)
Temporal	0.775 (0.058)	0.68 (0.49–0.83)	0.88 (0.77–0.95)	5.50 (2.75–11.01)	0.37 (0.29–0.62)	0.72 (0.53–0.87)	0.85 (0.74–0.93)
NS	0.840 (0.042)	0.61 (0.42–0.78)	0.92 (0.83–0.97)	7.97 (3.28–19.35)	0.42 (0.27–0.66)	0.79 (0.58–0.93)	0.83 (0.73–0.91)
TS	0.856 (0.039)	0.77 (0.59–0.90)	0.82 (0.70–0.90)	4.19 (2.43–7.23)	0.28 (0.14–0.54)	0.67 (0.49–0.81)	0.88 (0.77–0.95)
TI	0.921 (0.035)	0.90 (0.74–0.98)	0.89 (0.79–0.96)	8.39 (4.13–17.05)	0.11 (0.04–0.32)	0.80 (0.63–0.92)	0.95 (0.86–0.99)
NI	0.838 (0.040)	0.94 (0.79–0.99)	0.65 (0.52–0.76)	2.64 (1.88–3.72)	0.10 (0.03–0.39)	0.56 (0.41–0.70)	0.95 (0.85–0.99)

AUROC=area under receiver operating characteristic curve; CI=95% confidence interval; NI=infero-nasal; NLR=negative likelihood ratio; NPV=negative predictive value; NS=supero-nasal; PLR=positive likelihood ratio; PPV=positive predictive value; SE=standard error; TI=infero-temporal; TS=supero-temporal.